Chapter 4

EXTENSIONS OF THE IMPEDANCE-BASED STRUCTURAL HEALTH MONITORING TECHNIQUE

4.1 Extending technique to High Temperature Applications

4.1.1 Introduction

The objective of this chapter is to report the feasibility of using the impedance-based health monitoring technique for structures in an extremely high-temperature environment. The needs for on-line health monitoring system for these structures, such as steam pipes and boilers in power plants, are in great demand to avoid catastrophic failures. Currently, power plants rely on numerical methods and manual inspection to estimate the conditions of these structures, however, these techniques are not suitable for the prediction of incipient type of damage. A new approach using fiber-optic strain and temperature sensors was developed and investigated for power plant components and high-temperature applications, but ended in inconclusive results (Narendran and Weiss, 1996).

With the advent of commercialized high temperature piezoceramic materials (PZT), which have a Curie temperature higher than 1000 $^\circ C$, the implementation of the impedance method to the high temperature applications was worth of investigation. The impedance-based structural health monitoring technique has been successfully applied in the temperature range up to 75 $^\circ C$, however, the ability to detect damage under this extreme condition had not yet been tested. Therefore, as a proof of concept demonstration, experiments were performed to detect damage on a bolted joint structure in the temperature range of 500 – 600 $^\circ C$.

4.1.2 Experimental Setup

The experiment was conducted inside an oven equipped with a temperature controller. Using this controller, the temperature in the oven was raised to $600\,^{\circ}C$. A stainless steel bolted assembly is used in the experimental setup, as can be seen in Fig. 4.1. One PZT actuator/sensor patch (12x12x0.2 mm), obtained from Valpey-fisher Corporation, is bonded to the structure. This high-temperature piezoelectric material (Lithium Niobate) has a Curie temperature at $1150\ ^{\circ}C$. The material characteristics of this PZT are shown in Fig. 4.2. After the steady-state temperature had been reached, baseline readings have been taken for 7 days before the damage is induced in order to investige the variation of impedance curves. Damage was introduced by loosening the bolt by the small turn (60 degree turn) and electrical impedance measurements were repeated over the several frequency range. The HP 4194 impedance analyzer is used for the acquisition of electrical impedance.

Figure 4.1 Bolted joint used in the high temperature experiment

Because of the high temperatures involved in this experiment, extra care needs to be taken for the bonding and wiring of the PZT sensor/actuator. Several commericially-aviable adhesives were tested and Silver-epoxy and Platinum-epoxy are chosen to bond the PZT sensor, since they showed no cracking and debonding at the temperature above 600 $°C$. Also Platinum wires have been used for the connection between the PZT sensor and the impedance analyzer.

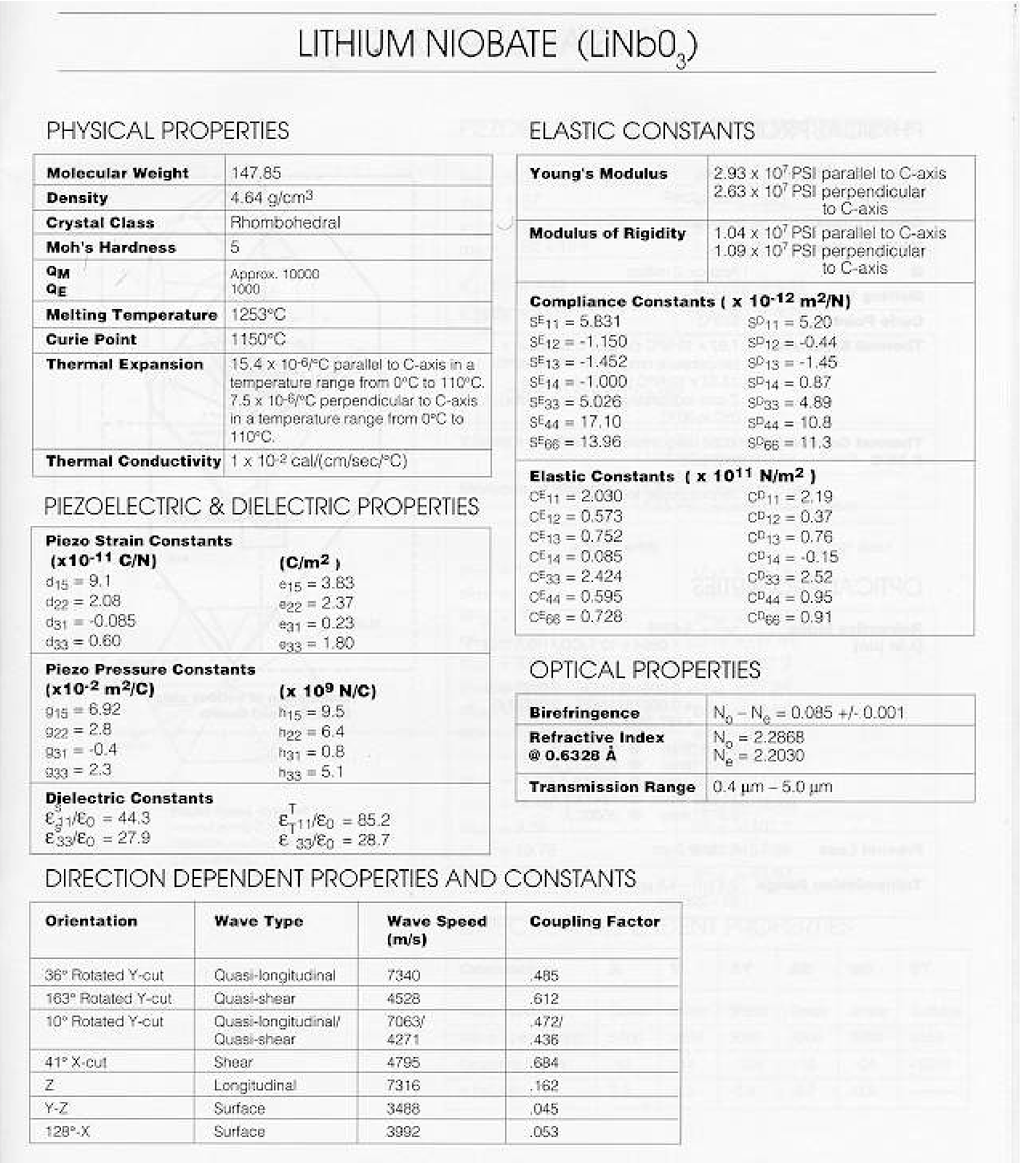

LITHIUM NIOBATE (LiNb0$_3$)

PHYSICAL PROPERTIES

Molecular Weight	147.85
Density	4.64 g/cm^3
Crystal Class	Rhombohedral
Moh's Hardness	5
Q_M **Q_E**	Approx. 10000 1000
Melting Temperature	1253°C
Curie Point	1150°C
Thermal Expansion	15.4 x 10^{-6}/°C parallel to C-axis in a temperature range from 0°C to 110°C. 7.5 x 10^{-6}/°C perpendicular to C-axis in a temperature range from 0°C to 110°C.
Thermal Conductivity	1 x 10^{-2} cal/(cm/sec/°C)

PIEZOELECTRIC & DIELECTRIC PROPERTIES

Piezo Strain Constants

(x10^{-11} C/N)	**(C/m^2)**
$d_{15} = 9.1$	$e_{15} = 3.83$
$d_{22} = 2.08$	$e_{22} = 2.37$
$d_{31} = -0.085$	$e_{31} = 0.23$
$d_{33} = 0.60$	$e_{33} = 1.80$

Piezo Pressure Constants

(x10^{-2} m^2/C)	**(x 10^9 N/C)**
$g_{15} = 6.92$	$h_{15} = 9.5$
$g_{22} = 2.8$	$h_{22} = 6.4$
$g_{31} = -0.4$	$h_{31} = 0.8$
$g_{33} = 2.3$	$h_{33} = 5.1$

Dielectric Constants

$\varepsilon^S_{11}/\varepsilon_0 = 44.3$	$\varepsilon^T_{11}/\varepsilon_0 = 85.2$
$\varepsilon^S_{33}/\varepsilon_0 = 27.9$	$\varepsilon^T_{33}/\varepsilon_0 = 28.7$

ELASTIC CONSTANTS

Young's Modulus	2.93 x 10^7 PSI parallel to C-axis 2.63 x 10^7 PSI perpendicular to C-axis
Modulus of Rigidity	1.04 x 10^7 PSI parallel to C-axis 1.09 x 10^7 PSI perpendicular to C-axis

Compliance Constants (x 10^{-12} m^2/N)

$s^E_{11} = 5.831$	$s^D_{11} = 5.20$
$s^E_{12} = -1.150$	$s^D_{12} = -0.44$
$s^E_{13} = -1.452$	$s^D_{13} = -1.45$
$s^E_{14} = -1.000$	$s^D_{14} = 0.87$
$s^E_{33} = 5.026$	$s^D_{33} = 4.89$
$s^E_{44} = 17.10$	$s^D_{44} = 10.8$
$s^E_{66} = 13.96$	$s^D_{66} = 11.3$

Elastic Constants (x 10^{11} N/m^2)

$c^E_{11} = 2.030$	$c^D_{11} = 2.19$
$c^E_{12} = 0.573$	$c^D_{12} = 0.37$
$c^E_{13} = 0.752$	$c^D_{13} = 0.76$
$c^E_{14} = 0.085$	$c^D_{14} = -0.15$
$c^E_{33} = 2.424$	$c^D_{33} = 2.52$
$c^E_{44} = 0.595$	$c^D_{44} = 0.95$
$c^E_{66} = 0.728$	$c^D_{66} = 0.91$

OPTICAL PROPERTIES

Birefringence	$N_o - N_e = 0.085$ +/- 0.001
Refractive Index @ 0.6328 Å	$N_o = 2.2868$ $N_e = 2.2030$
Transmission Range	0.4 μm – 5.0 μm

DIRECTION DEPENDENT PROPERTIES AND CONSTANTS

Orientation	**Wave Type**	**Wave Speed (m/s)**	**Coupling Factor**
36° Rotated Y-cut	Quasi-longitudinal	7340	.485
163° Rotated Y-cut	Quasi-shear	4528	.612
10° Rotated Y-cut	Quasi-longitudinal/ Quasi-shear	7063/ 4271	.472/ .436
41° X-cut	Shear	4795	.684
Z	Longitudinal	7316	.162
Y-Z	Surface	3488	.045
128°-X	Surface	3992	.053

Figure 4.2 The material Characteristics of Lithium Niobate used in the experiment.(Provided by Valpey-Fisher corporation)

4.1.3 Results and Analysis

The impedance measurements are shown in Fig 4.3, for visual comparison for both damaged and undamaged cases. It can be seen that the essential pattern of the impedance signatures remains the same over time before damage was induced. There are small random variations along the curves over the days of testing. However, the variations are relatively small and the measurements were repeatable. After the damage was induced, which is loosening one bolt (1/6 turn), a complete change occurs in the signature pattern of the impedance curve over the entire frequency range, as can be seen in Fig 4.3.

The variations of impedance signature in this experiment are relatively larger than those typically measured in room temperature. It is believed that, even though the measurements were taken after the steady state temperature has been reached, the variations come from the fact that a relatively large temperature fluctuation takes place inside the oven. However, when the damage metric charts are calculated, the values were seen to be small, as indicated in Fig. 4.4

It can be seen from damage metric charts that, at each measured frequency range, the largest metric from the variation has a value of lower than 50% when compared to the damage. This chart proves that the variation of the measurements, which is due to random uncontrollable effects, is small compared to a case when the structure is damaged. Note that the tightness of the bolt was maintained relatively high even after the damage was introduced, ensuring that damage is still in its incipient stage.

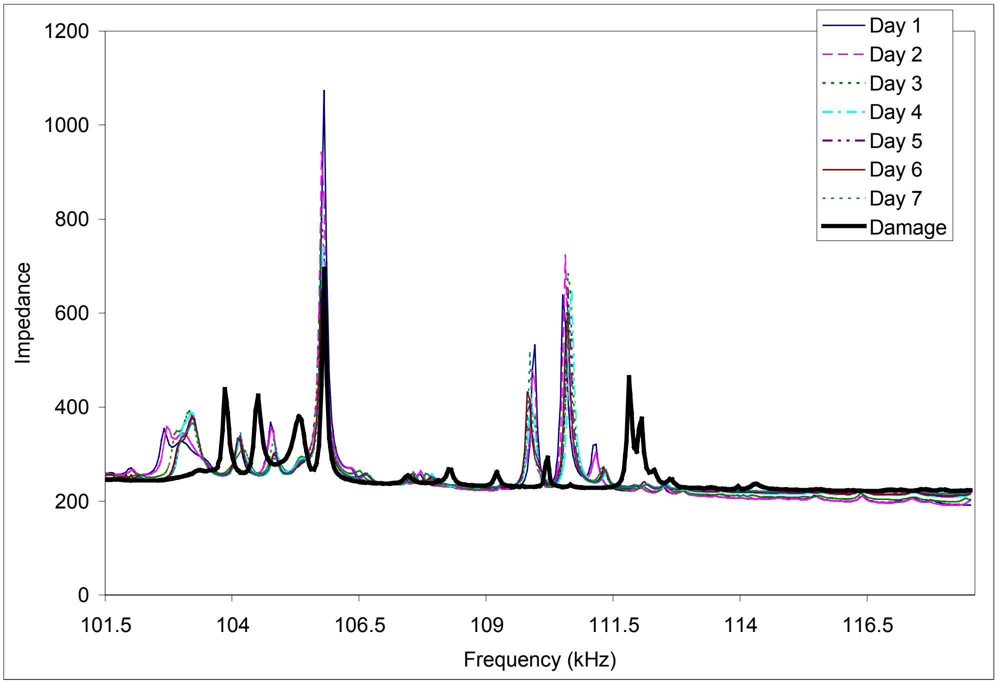

(a) Frequency Range of 100-115 kHz

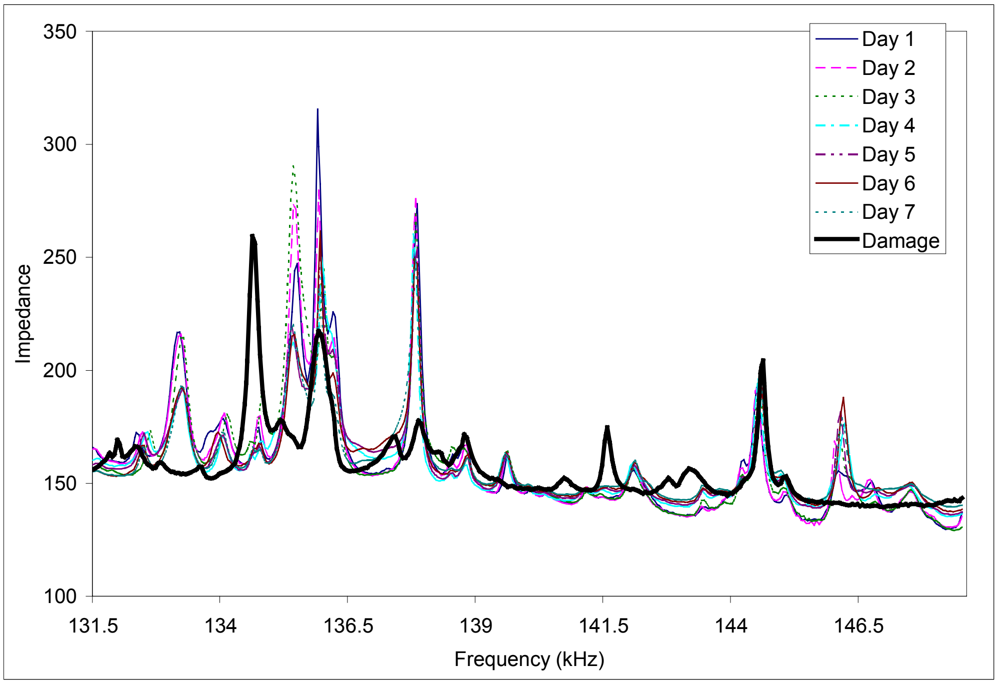

(b) Frequency Range of 130-150 kHz

Figure 4.3 The electrical impedance measurements at temperature 500 ℃

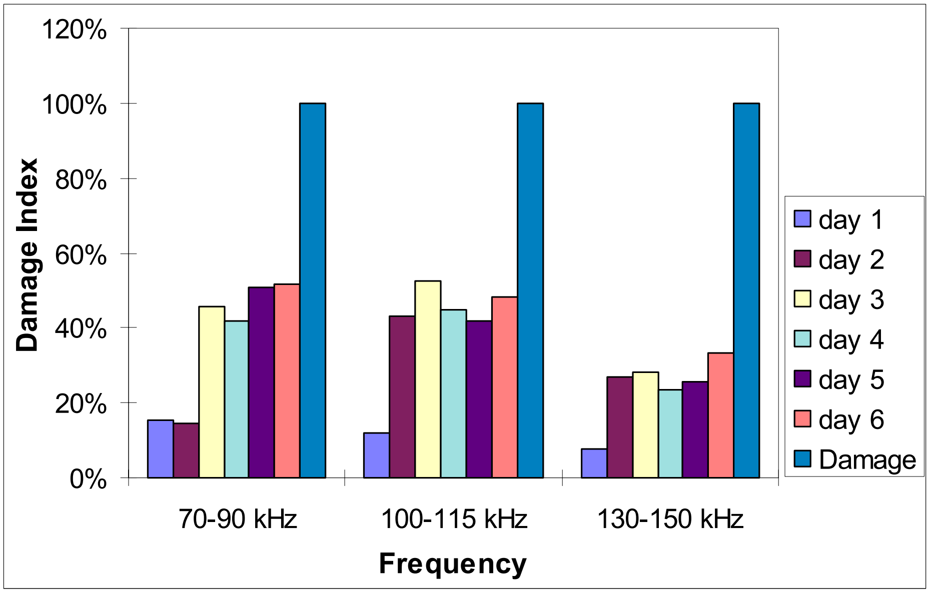

Figure 4.4 Damage metric chart over the different frequency range. Damage metrics are normalized against the value of damage.

4.1.4 Summary

The impedance-based structural health monitoring has been extended to detect damage under the high temperature environment. The proof-of-concept experiment demonstrates the capability of this method to monitor the integrity of high temperature structures. There are a number of practical field applications in which large temperature change can take place, such as power plant components and aerospace structures. The results presented in this chapter could provide an excellent example of the great potential of this impedance-based structural health monitoring technique to the wide variety of applications, even where the conventional NDE methods could not effectively approach the problem.

4.2 Health Assessments of Pipelines

4.2.1 Introduction

The objective of this research is to investigate the feasibility of using impedance-based health monitoring technique in monitoring critical civil facility, such as civil pipeline structures. This study is aimed to utilize the capability of this impedance method in identifying structural damage in those areas where a very quick condition monitoring is urgently needed, such as in a post-earthquake analysis of a hospital system.

Pipelines convey natural gas, oil, and water and some pipelines contain communications and power cables, which is very important to maintain functioning of residential and industrial activities. This facility is also required for the recovery action after natural disasters, such as an earthquake. However, pipelines are severely damaged by shaking, liquefaction and landslides during earthquakes (Airman and Muleski, 1981; O'Rourke and Palmer, 1996; Koseki *et al*., 1998) and the immediate assessment of pipeline facilities is critical to prevent fires, explosions, and pollution from broken gas or sewage lines. Although extensive research efforts have been focused on assessing the conditions of pipelines after earthquakes (Hwang *et al.,* 1998; Kitaura *et al*., 1998; Nyman *et al*., 1999), the condition monitoring of these structures is still based on limited information, without the definite means to assess the state of these structures.

This section describes the performance of the impedance-based technique in detecting real-time damage on a sample pipeline structures. Several conditions were imposed to simulate real-time damage, and the capability of the impedance method in tracking and monitoring the integrity of the typical civil facility has been demonstrated.

4.2.2 Experimental Setup

Bolted joints are commonly used to connect segmented piping lines. This interface can be the most critical source of failure of the pipelines, since significant ground movements can stress the joint beyond its yield or buckling capacity, while the main body of the pipe remains elastic (Eidinger, 1999). Therefore, the conditions of these joints need to be monitored to ensure the integrity of entire pipelines.

A model of pipelines with bolted joints is shown in Fig 4.5. This model consists of segmented pipes (d-40 mm), flanges, elbows and joints connected by more than 100 bolts. The size of this structure is 2 m wide and 1.3 m tall. PZT sensors/actuators are bonded on each joint to monitor the conditions of this structure. The HP4194 electrical impedance analyzer was used for the measurement of the PZT's electrical impedance in the frequency range of 80-100 kHz.

For this experiment, the total impedance of each junction (2 or 3 joints), labeled A to I, was utilized to track the damage. The total impedance refers to 'a single impedance signal acquiring from distributed PZTs'; the leads from the various distributed PZTs are physically connected together and this single lead is then connected to the terminal on the impedance analyzer. This procedure drastically reduces the interrogation time, as compared to that of analyzing each PZT separately. After measuring the baseline impedance signature, damage was introduced by loosening the bolts over several joints on this structure.

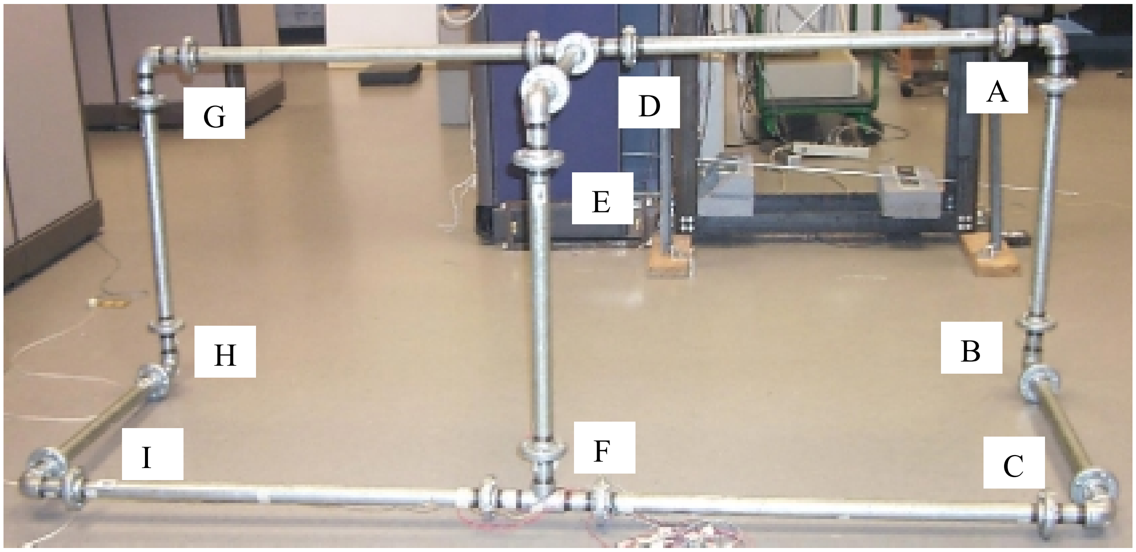

Figure 4.5 A pipeline used in the experiment

4.2.3 Experimental Results

The impedance measurements of PZTs at Junction D with 4 levels of local damage are shown in Fig 4.6. The bolts at Junction D were loosened as shown in labels. It can be seen from the figure that with increasing damage, the impedance signature shows a relatively large change in shapes. This change occurs because the damage modifies the apparent stiffness and damping of the joint. This variation shows the extreme sensitivity of the impedance-based method to the presence of damage in the sensing area. A damage metric chart is constructed in Fig 4.7. The damage metric charts quantify and summarize the information obtained from impedance response curves. As can be seen in the figure, with increase in extent of damage, there is a corresponding increase in the damage metric values. This chart provides a comprehensive and quick insight about the extent of damage and makes a quantitative comparison between different data sets.

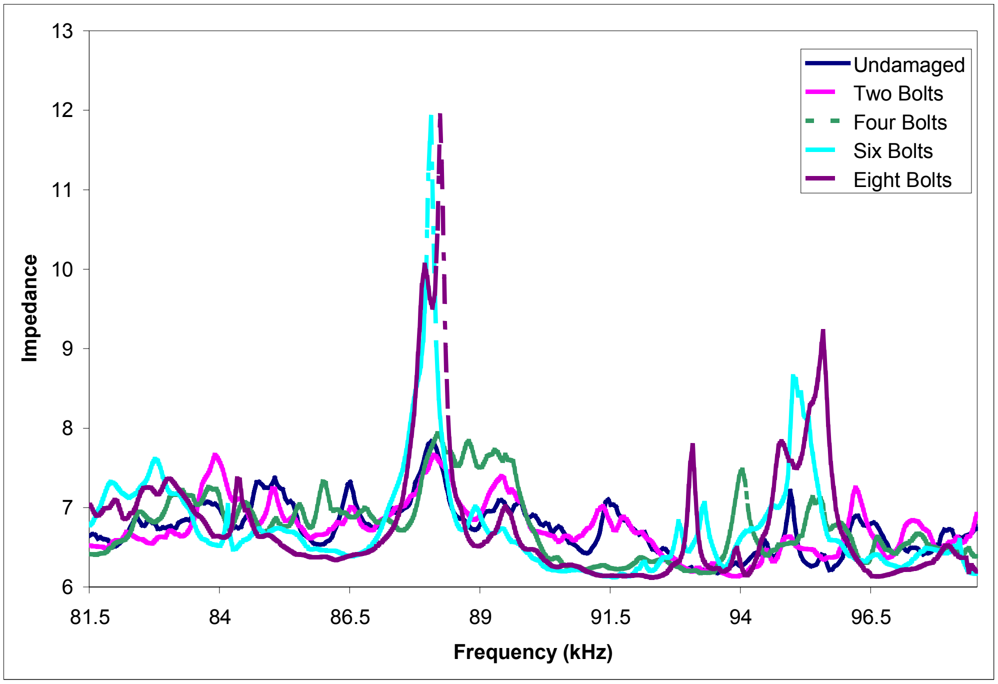

Figure 4.6 The electrical impedance measurements of PZTs at Junction D

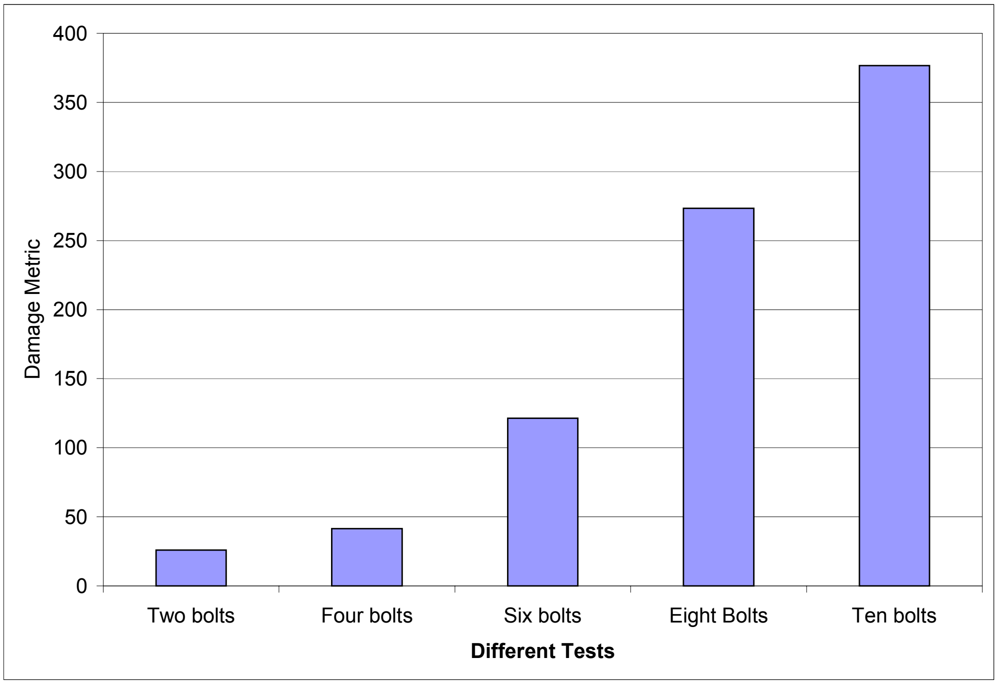

Figure 4.7 Damage Metric Chart. Comparison of metric values with induced damage

Another experiment was performed in the global scale. The three conditions were imposed to this structure in sequence, as shown below.

- Damage I : loosening 3 bolts at Junction A and B, respectively
- Damage II : loosening 2 bolts at Junction E and G, respectively
- Damage III : loosening 4 bolts at Junction F, G and H, respectively

The impedance measurements of PZTs located at junction B is shown in Fig 4.8. For the junction B, when Damage I was introduced, the measurement is significantly different from the baseline measurement, which is indicative of imminent damage. However, the other two damage conditions were imposed, the remaining curves follow the same pattern as that of the second reading, since those are well out of sensing range of PZTs located at junction B. Another impedance measurements of junction G are shown in figure 4.9. The location of Damage I is out of sensing range of PZTs, hence almost no change in impedance signature was observed. However, when Damage II and III were introduced, the measurements show significant changes in signature patterns.

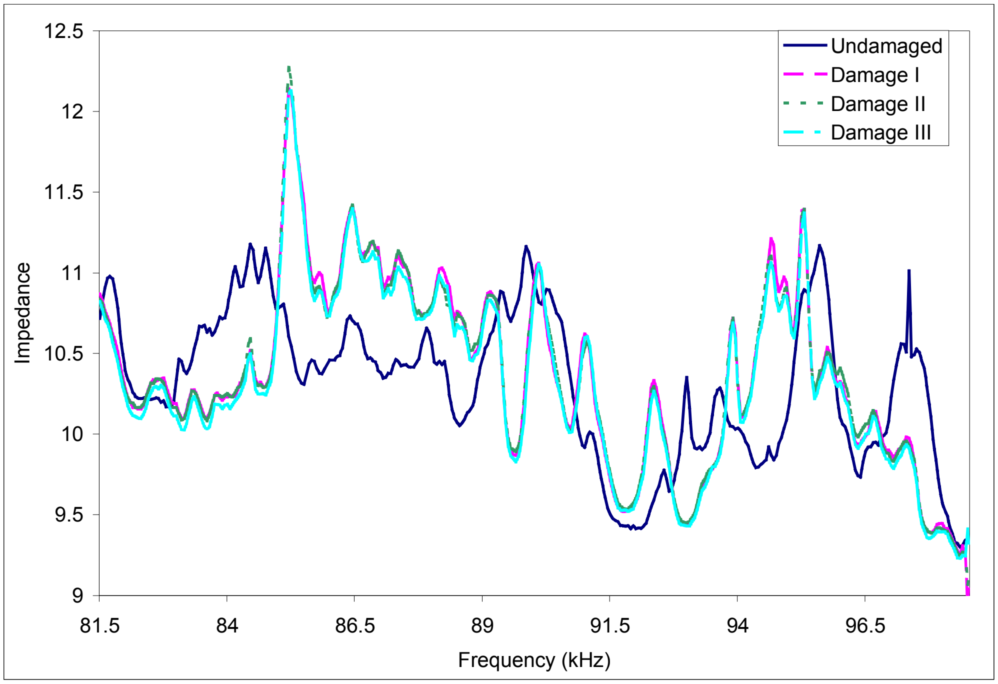

Figure 4.8 The electrical impedance measurements of PZTs at Junction B

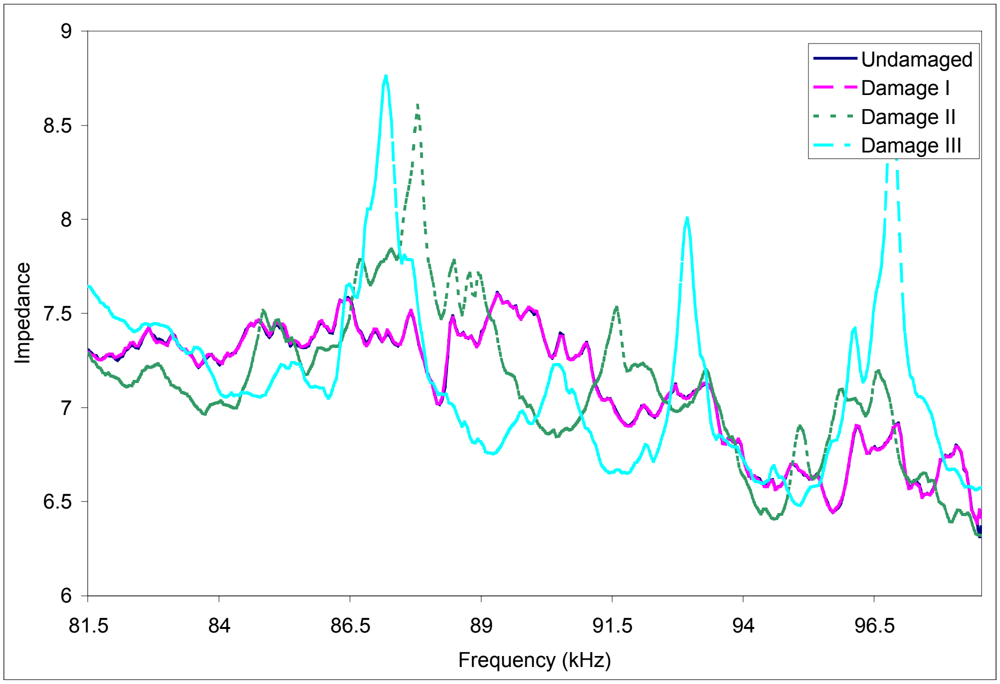

Figure 4.9 The electrical impedance measurements of PZTs at Junction G

Damage metric charts demonstrates the results more clearly, as can be seen in Figure 4.10. It can be seen that at Damage I, there is a large increase in the damage metric value for PZTs at A and B. The other PZTs show a very small change in damage metric, this is because they are distant from the damage. Similar results were obtained when damage II and III were induced. Each PZT shows an increase in damage metric value, if damage is induced close to the sensors.

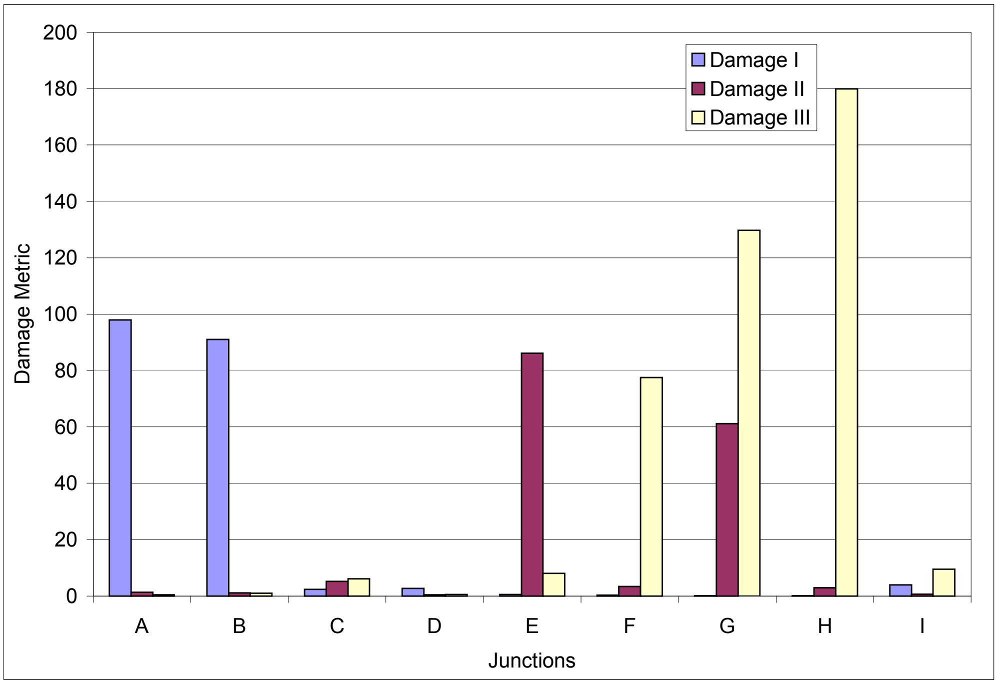

Figure 4.10 Damage metric chart for different locations.

4.2.4 Summary

This piping structure provided an excellent experiment to study the detection of imminent damage in pipeline structures. It can be seen from the observations and charts that the location of the damage can be accurately predicted. Multiple damages in different areas are picked up accurately. The use of the damage metric charts in providing a quick, accurate summary of the health of the structure became obvious during the testing. The time necessary to take the impedance measurements and to construct the damage metric is less than 5 minutes, which is quick enough for an on-line implementation of this technique for the post-event condition assessment.

4.3 Conclusion

The impedance-based health monitoring technique has been extended to detect real-time damage in the high temperature structures. The proof-of–concept demonstration provided an insight into the critical aspects of the full-scale development of high-temperature structural health monitoring system. The hot, dirty environments of high temperature applications impose difficulties on estimating and maintaining the durability of bonding between PZT sensors and structures, and wiring of PZT sensors. The long-term reliability of the piezoelectric under the extreme condition has not yet been fully tested and is beyond the scope of this research. Nevertheless, the impedance-based health monitoring technique shows its potential to monitor the structure under the extremely high temperature conditions, well above 500 $°C$.

To demonstrate the capability of the impedance-based technique on the civil pipeline structures, experimental investigations were performed. This impedance-based technique has demonstrated its great potential to be used for the post-event condition assessment, because of its ability of quick assessment of the structures. The condition assessment can be made immediately after a natural hazard, since the time necessary to interrogate the PZTs and to interpret the outputs of this method is quick enough for on-line implementation.